C: Surfaces, Interfaces, Porous Materials, and Catalysis

Surface Passivation and Positive Band-Edge Shift of p-Si(111) Surfaces Functionalized with Mixed Methyl/Trifluoromethylphenylacetylene Overlayers

Miguel Cabán-Acevedo, Kimberly M. Papadantonakis, Bruce S. Brunschwig, and Nathan S. Lewis

J. Phys. Chem. C, **Just Accepted Manuscript** • DOI: 10.1021/acs.jpcc.0c02017 • Publication Date (Web): 30 Jun 2020

Surface Passivation and Positive Band-Edge Shift of p-Si(111) Surfaces Functionalized with Mixed Methyl/ Trifluoromethylphenylacetylene Overlayers

Miguel Cabán-Acevedo,† Kimberly M. Papadantonakis, Bruce S. Brunschwig,‡ Nathan S. Lewis*,†,‡

†Division of Chemistry and Chemical Engineering, and ‡Beckman Institute, California Institute of Technology, Pasadena, California 91125, United States

ABSTRACT. Chemical functionalization of semiconductor surfaces can provide high-efficiency photoelectrochemical devices through molecular-level control of the energetics, surface dipole, surface electronic defects, and chemical reactivity at semiconductor/electrolyte junctions. We describe the covalent functionalization by nucleophilic addition chemistry of p-Si(111) surfaces to produce mixed overlayers of trifluoromethylphenylacetylene (TFMPA) and methyl moieties. Functionalization of Cl-terminated Si(111) surfaces with TFMPA moieties introduced a positive surface molecular dipole that in contact with CH_3CN or Hg produced a positive band-edge shift of the semiconductor relative to junctions with CH_3-Si(111) surfaces. Methylation of the Cl/TFMPA surfaces using methylmagnesium chloride resulted in the degradation of the TFMPA moieties, whereas methylation using methylzinc chloride allowed controlled production of mixed TFMPA/methyl-terminated surfaces and permitted reversal of the order of the functionalization steps so that nucleophilic addition of TFMPA could be accomplished after methylation of Cl-Si(111) surfaces. Mixed TFMPA/methyl functionalization resulted in a Si(111) surface with surface recombination velocities of 2×10^2 cm s^{-1} that exhibited an ~ 150 mV positive band-edge shift relative to CH_3-Si(111) surfaces.

I. INTRODUCTION

Chemical functionalization of semiconductor surfaces is a powerful route to high-efficiency photoelectrochemical devices through simultaneous molecular-level control of the energetics, surface electronic defects, and chemical reactivity of semiconductor/liquid junctions. Introduction of a dipole on the surface of a covalent semiconductor, such as Si, through functionalization of the surface by a thin organic monolayer can shift the energy-band positions of the semiconductor relative to the contacting phase (Figure 1).[1-5] Band-alignment requirements and sensitivity to electronic defects at the semiconductor surface place substantial limitations on the use and efficiency of semiconductor/electrolyte junctions.[6]

Theoretical and experimental studies on Si suggest that the direction and magnitude of the surface dipole moment is dependent on the molecular dipole properties of the attached group.[1] Covalent surface functionalization has been demonstrated for an extensive variety of semiconducting inorganic 3D substrates such as Si, Ge, diamond, GaAs, TiO_2, and $GaInP_2$.[7-16] For a photocathode in contact with a redox couple in solution, the potential of the conduction-band edge (E_{cb}) of the semiconductor must be more negative than the electrochemical potential of the contacting phase prior to equilibration; however, for high-efficiency photoconversion the difference between the Fermi-level potential of the semiconductor (E_F) and that of the contacting phase needs to be maximized.[17]

Halogenation of H-Si(111) surfaces followed by alkylation with methylmagnesium chloride[18] results in a fully methyl-terminated (CH_3-Si(111)) surface that has a low surface recombination velocity (~ 20 cm s^{-1}) and extended stability (> 500 h) in air.[19-22] Compared to hydrogen-terminated (H-Si(111)) surfaces, CH_3-Si(111) surfaces are chemically robust and can be interfaced with metals without the formation of deleterious metal silicides.[23-25] A negative surface dipole shift of up to ~ -0.8 V has been observed for junctions between Hg and CH_3-Si(111) relative to H-Si(111).[23] A negative surface dipole shifts the conduction and valence bands to more negative potentials (electron energies closer to the vacuum level) relative to the chemical potential of a contacting phase. This shift increases the built-in voltage, V_{bi}, and improves the band alignment of n-type silicon devices (Figure 1a-c). In contrast, a negative dipole shift reduces the band bending and built-in voltage ($V_{bi} = E_F - E(A/A^-)$) for contacts to p-type silicon, and a positive surface dipole is therefore required to position the semiconductor bands to more positive potentials relative to the contacting phase and therefore produce improved photovoltages for p-type photocathodes (Figure 1d-f).

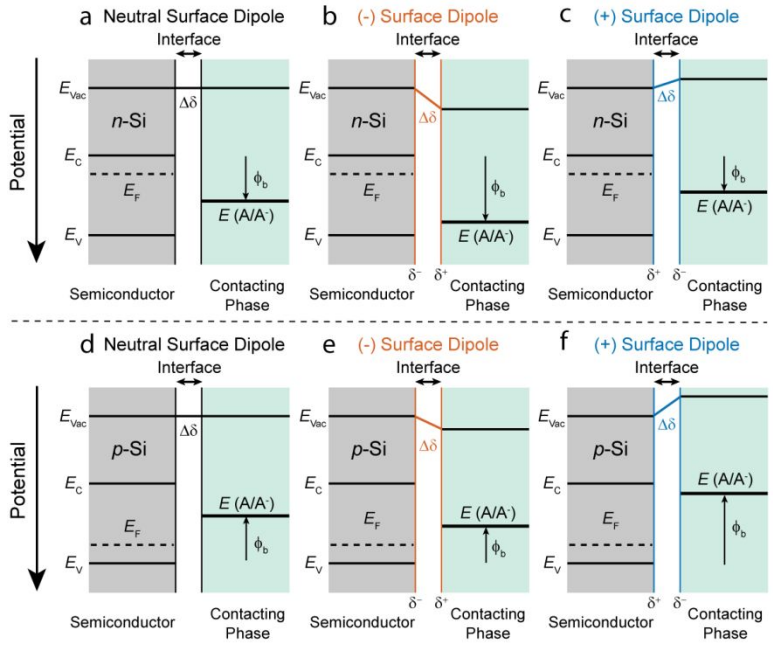

Figure 1. Diagram illustrating the shift in the relative positions of the bands for (a, b, c) n-type and (d, e, f) p-type semiconductor, and the contacting electrolyte layer induced by (a, d) no, (b, e) negative, and (c, f) positive dipole layers. In this figure, E_C, E_V, E_F, and E_{Vac} represent the potentials of the conduction-band-edge minimum, valence-band-edge maximum, Fermi-level and the vacuum level, respectively. The shift in the vacuum level caused by the electric field within the dipole layer is represented as $\Delta\delta$. The barrier height, ϕ_b, limits the attainable photovoltage.

Chemical modification with mixed organic moieties is a promising strategy to functionalize inorganic semiconducting surfaces when chemical passivation and target functionality cannot be achieved by a single moiety, or when multiple chemical functionalities are needed.[5, 12, 20, 26-28] In the case of Si(111), favorable band-edge positions have been obtained by functionalizing p-Si with 3,4,5-trifluorophenylacetylene (TFPA), an organic moiety with a positive molecular dipole.[11, 29] Phenyl groups are sterically prevented from binding to every Si atom on the Si(111) surface,[30] so the p-Si(111) samples were sequentially functionalized with TFPA, to induce the desired dipole, and then with methyl groups, to passivate surface sites not bound to TFPA. Mixing TFPA and methyl-terminated sites resulted in a net positive band-edge shift relative to CH_3-Si(111) surfaces and encouragingly reversed the sign of the dipole relative to CH_3-Si(111) surfaces. However, for photoelectrochemical junctions in acetonitrile, the mixed TFPA/methyl-functionalized p-Si surfaces displayed low energy-conversion efficiencies and yielded photovoltages that were not commensurate with the measured changes in barrier height. The suboptimal photoelectrochemical properties of mixed TFPA/methyl-functionalized surfaces have been attributed to a relatively high surface recombination velocity (1900 cm s^{-1} for optimal TFPA coverage), implying that for high-efficiency junctions defect passivation is required in addition to a favorable energy-band alignment.

We describe herein a synthetic pathway to p-Si(111) surfaces functionalized with a mixed overlayer containing 4-trifluoromethylphenylacetylene (TFMPA) and methyl groups. The resulting surfaces exhibit a tunable, positive surface dipole beneficial for use of p-Si(111) photocathodes, and additionally yields surfaces that have high degrees of electrical passivation. Fluoro (–F) groups have a substantially larger ionic radius than hydrogen (–H) groups, so the –F groups arranged in a single *para*-trifluoromethyl (CF_3) group, as opposed to the –F groups in *para*- and *meta*- phenyl positions on TFPA, reduce intermolecular steric hindrance and allow an increase in the surface packing density for TFMPA relative to TFPA. Consequently, a stronger positive dipole should be induced along with a reduction of unreacted surficial defect sites. The functionalized p-Si(111) surfaces were characterized by transmission infrared spectroscopy (TIRS) and X-ray photoelectron spectroscopy (XPS). The energy-band alignment was determined for Hg junctions to the functionalized p-Si(111) surfaces, in conjunction with measurements of surface recombination velocities. Additionally, the photoelectrochemical behavior of semiconductor/electrolyte junctions was evaluated for mixed TFMPA/methyl-functionalized Si(111) surfaces in contact with CH_3CN solutions containing a range of one-electron, reversible, outer-sphere redox couples.

II. EXPERIMENTAL SECTION

Scheme 1. (a) Synthesis of hydrogen-, chlorine-, methyl-, and (b) mixed TFMPA/methyl-terminated silicon surfaces. (c) Trend in reactivity for different organometallic methyl nucleophiles.

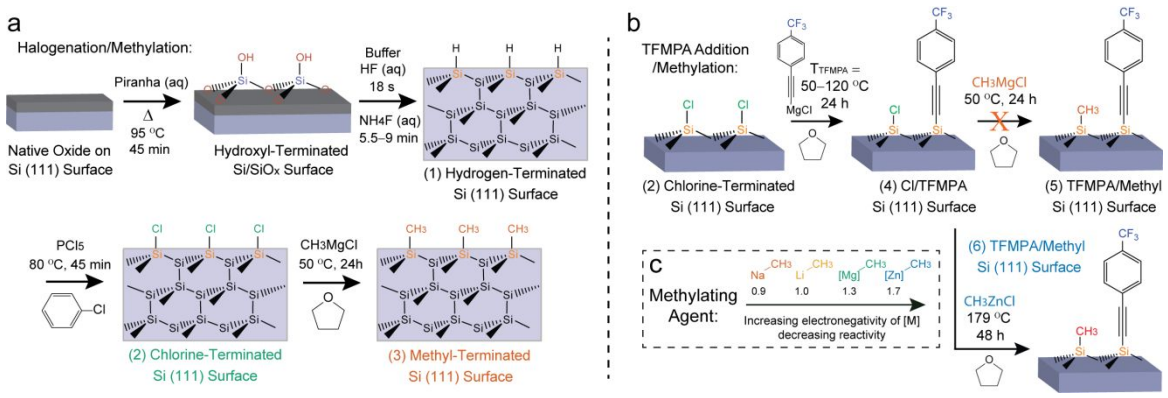

II.A. Materials and Methods for Surface Functionalization of Silicon. Water with a resistivity ≥ 18.2 MΩ·cm was obtained from a Barnstead E-Pure system. Aqueous ammonium fluoride (NH_4F(aq), 40% by weight (11 M) semiconductor grade, Transene Company Inc., Danvers, MA) was purged prior to use by bubbling for ~ 45–60 min with Ar(g) (ultra-high-purity grade, 99.999%, Airgas). All oxygen- or water-sensitive chemicals were stored and handled in a N_2(g)-purged glovebox (<4 ppm O_2(g)). All other chemicals were used as received.

Silicon wafers used herein had a miscut orientation within 0.5° of the (111) crystal plane. Surface characterization measurements, including transmission infrared spectroscopy, X-ray photoelectron spectroscopy, and time-resolved microwave conductivity, were performed on float-zone-grown Si wafers (University Wafer, Boston, MA) that were double-side polished, 450 ± 10 μm in thickness, unintentionally doped, and 5–5.5 kΩ·cm in resistivity. Electrical and photoelectrochemical measurements were performed on Czochralski-grown p-Si wafers (Addison Engineering, San Jose, CA) that were double-side polished, 300 ± 25 μm in thickness, and doped with boron to a resistivity of 0.3 to 0.43 Ω·cm. Prior to surface functionalization, an ohmic back contact was formed by deposition and thermal diffusion of aluminum onto one side of the p-Si wafers. Deposition was performed by radio-frequency sputtering of an Al target at 150 W for 45 min using an AJA Orion sputtering system. During deposition, the plasma was sustained by flowing 20 sccm of Ar(g). The chamber pressure was 5 mTorr during the deposition, and the base pressure of the chamber was < 10^{-7} Torr prior to deposition. The thickness of the aluminum film was measured as ~ 100 nm by profilometry (using a DektakXT profilometer). After deposition, the sputtered wafer was annealed in forming gas (5% H_2(g) in N_2(g)) at 800 °C for 20 min using a tube furnace.

II.A.1. Synthesis of Hydrogen-Terminated Si(111) Surfaces (Scheme 1.a.1). In a typical reaction, silicon wafers were first cut into rectangular pieces with dimensions of 1.3 × 3.2 cm and subsequently sonicated in methanol and in water for 10 min each, to remove particulates and debris. After sonication, the substrates were dried under a stream of Ar(g). The rectangular silicon substrates were then etched for 10 min with a piranha solution composed of a 3:1 (v:v) ratio of 18 M sulfuric acid (95-98% v/v, ACS Grade, EMD) to 8.8 M (30% wt. in H_2O) hydrogen peroxide (ACS grade, EMD) at a temperature of 95 ± 5 °C using a heated water bath. After etching in the piranha solution, the substrates were thoroughly rinsed with water for 1–2 min and were then dried under a stream of Ar(g). Piranha etching removes adventitious organic surface species and induces surface oxidation, resulting in the formation of a hydrophilic hydroxyl-terminated silicon oxide surface layer. The resulting surface oxide layer was removed by isotropic etching for 18 s with buffered hydrofluoric acid (semiconductor grade, Transene Company Inc., Danvers, MA). The substrates were then briefly rinsed with water for a few seconds and dried with Ar(g). After one additional repetition of the piranha and buffered HF(aq) etching steps, the rectangular silicon substrates were etched anisotropically for 5.5–9 min with Ar(g)-purged 40% NH_4F(aq), followed by a brief water rinse and drying under a flow of Ar(g), resulting in atomically flat hydrogen-terminated silicon(111) surfaces.[21, 31-32]

II.A.2. Synthesis of Chlorine-Terminated Si(111) Surfaces (Scheme 1.a.2). Atomically flat H-Si(111) substrates were quickly transferred to a N_2(g)-purged glovebox (< 4 ppm O_2(g)) and subsequently rinsed with chlorobenzene (anhydrous, ≥99.8%, Sigma-Aldrich). The H-Si(111) substrates were then submerged in a chlorobenzene solution saturated with phosphorus(V) pentachloride (PCl_5, ≥99.998% metal basis, Alfa Aesar) and heated to 80 °C (measured with a thermocouple) for 45 min, using a custom dry block heater, to chlorinate the surface.[18, 33] At the end of the reaction, the Cl-terminated Si(111) substrates were removed from the chlorobenzene solution and thoroughly rinsed with chlorobenzene and then with tetrahydrofuran (THF, anhydrous, inhibitor-free, ≥99.9%, Sigma-Aldrich).

II.A.3. Synthesis of Methyl-Terminated Si(111) Surfaces (Scheme 1.a.3). Cl-terminated Si(111) surfaces were methylated with a 3 M solution of methylmagnesium chloride (CH_3MgCl, Sigma-Aldrich) in THF for 24 h at 50 °C using a custom dry block heater.[18] At the end of the reaction, the methyl-terminated silicon substrates were removed from the methylating solution, thoroughly rinsed with THF, and transferred out of the glovebox in a test tube that contained fresh THF. The substrates were then sonicated in THF, in methanol, and in water, for 10 min each. After sonication, the methyl-terminated silicon substrates were blown dry with Ar(g).

II.A.4. Nucleophilic Addition of 4-(trifluoromethyl)phenylacetylene (TFMPA) (Scheme 1.b.4). Cl-terminated silicon substrates were submerged in a 0.2 M solution of TFMPA magnesium chloride in THF and heated to 50–120 °C for 24 h using a home-built dry block heater. Prior to the reaction, the TFMPA magnesium chloride nucleophile was freshly generated by deprotonation of TFMPA (97%, Sigma-Aldrich) with a stoichiometric amount of CH_3MgCl at room temperature. For nucleophilic addition performed at

temperatures > 60 °C, the reaction was carried out in a glass pressure vessel (heavy walled glass tube, 10.2 cm long × 8 mm outer diameter, PTFE plug with back seal O-ring, Ace Glass). After reaction, the mixed Cl/TFMPA-terminated substrates were removed from solution and thoroughly rinsed with THF.

II.A.5. Synthesis of Mixed TFMPA and Methyl-terminated Si(111) Surfaces (Scheme 1.b.6). Mixed Cl/TFMPA-terminated silicon substrates were methylated with a 1 M solution of methylzinc chloride (CH_3ZnCl, Sigma-Aldrich or Acros Organics) in THF for 48 h at a temperature of ~ 179 °C (measured with a thermocouple) using a custom dry block heater. The reaction was performed in a glass pressure vessel (heavy-walled glass tube, 20.3 cm long × 8 mm outer diameter, PTFE plug with back seal O-ring, Ace Glass) due to the high vapor pressure of THF at the reaction temperature. *Note that appropriate safety precautions must be taken due to the potential explosion risk posed by the high pressure built up inside of the reaction vessel.* At the end of the reaction time, the mixed TFMPA/methyl-terminated silicon substrates were removed from the methylating solution, thoroughly rinsed with THF, and transferred out of the glovebox in a test tube containing THF. The substrates were then sonicated in THF, in methanol, and in water for 10 min each. After sonication, the mixed TFMPA/methyl-terminated silicon substrates were blown dry with Ar(g).

II.B. Surface Characterization Methods. *II.B.1. Transmission Infrared Spectroscopy (TIRS).* TIRS spectra were collected using a Thermo Scientific Nicolet 6700 optical spectrometer equipped with a deuterated L-alanine-doped triglycine sulfate (DLaTGS) detector, an electronically temperature-controlled (ETC) EverGlo mid-IR source, a N_2(g) purge, and a KBr beam splitter. Functionalized silicon wafers (1.3 × 3.2 cm) were mounted with the incident IR beam at 30º or 74° (Brewster's Angle for silicon at ~1,500 cm^{-1}) with respect to the surface normal, using a custom-built attachment. Spectra collected at 30° show modes primarily parallel to the surface, while those collected at 74° show modes primarily perpendicular to the surface because the transmitted light has little intensity polarized parallel to the surface.[21, 34] Reported spectra are averages of 1500 scans at 4 cm^{-1} resolution. After data collection, spectra were ratioed using the corresponding H-terminated surface as the background, which was measured prior to functionalization. The baseline was flattened if needed, and the residual peaks due to water and the atmosphere were subtracted. TIRS data collection and processing were performed using OMNIC software v.9.2.41.

Ab initio molecular quantum chemical calculations of infrared vibrational frequency modes for gas-phase TFMPA and TFMPA-TTMSS were performed using the GAMESS(US) 2018 R1 simulation package.[35-36] Calculations were performed by applying the density-functional-theory (DFT) method, with the B3LYP functional and the 6-311^{++}G (*d*, *p*) basis set. Using the vibrational frequency results for gas-phase TFMPA and TFMPA-TTMSS, a corresponding infrared spectrum was simulated using GaussSum.[37] The simulated IR spectra for TFMPA were utilized only to semi-quantitatively corroborate the chemical identity of the observed experimental peaks.

II.B.2. X-ray Photoelectron Spectroscopy (XPS). XPS data were collected using a Kratos AXIS Ultra spectrometer. The instrument was equipped with a hybrid magnetic and electrostatic electron-lens system, a delay-line detector (DLD), and a monochromatic Al Kα X-ray source (1486.7 eV). Spectra were collected at pressures < 9×10^{-9} Torr and using a photoelectron-ejection vector (take-off angle) of 90° with respect to the sample surface plane. The aperture of the electron-collection lens was set to sample a 700 × 300 μm spot, and the analyzer pass energy was 80 eV for survey spectra and 10 eV for high-resolution spectra. The energy scale and work function for the instrument were calibrated using clean Au, Ag, and Cu standards. The instrument was operated using Vision Manager software v.2.2.10 revision 5.

II.B.3. Time-Resolved Microwave Conductivity. Surface recombination velocity (*S*) measurements were performed using a contactless time-resolved microwave conductivity apparatus. Electron−hole pairs were generated on the functionalized silicon substrates by irradiation with a 20 ns laser pulse at 905 nm. The laser pulse was produced by an OSRAM laser diode and an ETX-10A-93 driver. The charge-carrier lifetime was determined by monitoring the change in reflected microwave intensity using a PIN diode connected to an oscilloscope. The data were collected using a custom LabView program.

II.B.4. Electrical Characterization in Contact with Hg drop. Electrical characterization measurements in contact with Hg (electronic grade, 99.9999% trace metal basis, Alfa Aesar) were performed inside an Ar(g)-filled glovebox (<0.3 ppm O_2(g)) at room temperature. Functionalized p-Si substrates (with dimensions of 1 × 1.3 cm) were placed on a polished Cu plate (with Ga/In eutectic as a contact between the substrate and the Cu plate), and a cylindrical Teflon cell was placed on top of the substrate to confine the electrode area to 0.314 cm^2. Hg was then added to the Teflon cell to cover the exposed area of the substrate, and a Pt wire was used to contact the top of the Hg drop.

Electrical measurements were collected using a Biologic SP-300 potentiostat in a two-electrode configuration, with the Cu plate connected as the working electrode and the Pt wire as the counter electrode. Current density versus applied voltage (J−V) measurements were performed from −0.5 to +0.5 V at a scan rate of 20 mV s^{-1}. Impedance spectroscopy was performed using a sinusoidal AC probe with an amplitude of 10 mV and under an applied DC voltage window ranging from 0 to −0.5 V. The applied DC voltage window was divided in 30 voltage steps. At each voltage step, the frequency of the AC probe was varied from 1 MHz to 1 Hz, and impedance data were collected every 12 points per decade after averaging 3 consecutive measurements at each point. The dependence of the differential capacitance (C_d) on the applied voltage (C_d −V) of the functionalized substrates was obtained by fitting the impedance data in the high-frequency region (located within the 10 Hz to 100 KHz range) that had phase-angle values > 80° to a simplified Randles circuit. The C_d −V data are reported herein in the form of Mott-Schottky plots ($1/C_d^2$−V).

II.C. Photoelectrochemical Methods. *II.C.1. Electrode Fabrication.* Silicon working electrodes were fabricated by affixing the coiled end of tinned Cu wires to the back side (i.e. the side with the diffused Al contact) of functionalized p-Si substrates using Ga/In eutectic and conductive silver paint (Ted Pella Inc.). The Cu was then electrically isolated by mounting each substrate to a borosilicate

glass tube using Loctite Hysol 9460 (insulating epoxy). After fabrication, the working electrodes were placed overnight in an air-filled desiccator to cure the insulating epoxy. The active geometric area (area of the surface not covered by the insulating epoxy) of the functionalized silicon working electrodes was 0.1–0.2 cm^2. Prior to use, Pt wire and Pt mesh electrodes were chemically etched with a 3:1 ratio of concentrated hydrochloric acid to concentrated nitric acid (aqua regia).

Ag^+/Ag reference electrodes were freshly prepared using borosilicate tubing, Vycor 7930 porous glass frits (CH Instruments Inc.), and Teflon heat-shrink tubing. The filling solution consisted of ~ 10 mM silver nitrate ($AgNO_3$, CH Instruments Inc.) and 1.0 M lithium perchlorate in dry acetonitrile. The Ag wire (0.5 mm diameter, ≥99.99%, Sigma-Aldrich) was polished with silicon carbide sandpaper, thoroughly rinsed with water, and transferred immediately to an Ar(g)-filled dry glovebox.

II.C.1. Redox Couples. A series of one-electron redox couples having a Nernstian potential of $E(A/A^-)$ was used to probe the dependence of the open-circuit voltage of functionalized silicon substrates on the solution potential (see Table S1).[38] Cobaltocene (Cp_2Co, bis(cyclopentadienyl)cobalt(II), 98%, Strem) and decamethylcobaltocene (Cp^*_2Co, bis(pentamethylcyclopentadienyl)cobalt(II), 98%, Strem) were purified by vacuum sublimation. The cobalt salts cobaltocenium ($Cp_2Co^+PF_6^-$, bis(cyclopentadienyl)cobaltocenium hexafluorophosphate, 98%, Strem) and decamethylcobaltocenium ($Cp_2{}^*Co^+PF_6^-$, bis(pentamethylcyclopentadienyl)cobaltocenium hexafluorophosphate, 98%, Sigma-Aldrich) were recrystallized from an ethanol (ACS grade, EMD)/acetonitrile (ACS grade, EMD) solution and dried under vacuum. The reduced species 1,1′-dicarbomethoxycobaltocene ($(CpCO_2CH_3)_2Co$, 1,1′-bis(η⁵-methoxycarbonylcyclopentadienyl)cobalt) was synthesized by reacting cobalt chloride ($CoCl_2$, 99.999% trace metals basis, Sigma-Aldrich) with sodium cyclopentadienide,[39-40] and the oxidized ($(CpCO_2CH_3)_2Co^+$) species was generated in situ by electrolysis. Methyl viologen (MV^{2+}, 1,1′-dimethyl-4,4′-bipyridiniumhexafluorophosphate) was prepared according to a literature procedure.[41] The reduced species $MV^{+\bullet}$ was generated by electrolysis of MV^{2+} at −0.85 V *vs* the Ag^+/Ag reference electrode. Subsequent in situ generation of $MV^{+\bullet}$ was performed to maintain the cell potential within 25 mV of the initial measured open-circuit potential.

The reduced species octamethylnickelocene (Me_8Cp_2Ni, bis(tetramethylcyclopentadienyl)nickel, 98%, Strem) was purified by sublimation, and the oxidized ($Me_8Cp_2Ni^+$) species was generated *in situ* by electrolysis. The reduced iron complexes, decamethylferrocene (Cp^*_2Fe, bis(pentamethylcyclopentadienyl)iron, 99%, Strem) and ferrocene (Cp_2Fe, bis(cyclopentadienyl)iron, 99%, Strem), were purified by sublimation. The iron salt decamethylferrocenium ($Cp^*_2Fe^+BF_4^-$, bis(pentamethylcyclopentadienyl)ferrocenium tetrafluoroborate) was generated by oxidation of the neutral metallocene, whereas ferrocenium tetrafluoroborate ($Cp_2Fe^+BF_4^-$, bis(cyclopentadienyl)iron(III) tetrafluoroborate, technical grade, Sigma-Aldrich) was purified by recrystallization.

Electrolysis was performed using a Pt mesh working electrode in the main electrochemical cell compartment and a Pt mesh counter electrode in a compartment separated by an electro-porous KT glass frit (Koslow Scientific Co.). The Nernstian potential of the solution was determined by cyclic voltammetric (CV) measurements using a Pt wire as the working electrode and Ag^+/Ag as the reference electrode. At the end of a set of experiments, the Ag^+/Ag reference electrode was calibrated with respect to the formal reduction potential (E^0) of ferrocene$^{0/+}$.

II.C.2. Photoelectrochemical Measurements. Open-circuit voltage (V_{oc}) and current density versus potential (J–E) measurements were collected in a four-port, cylindrical, flat-bottomed, borosilicate cell that contained 1.0 M lithium perchlorate ($LiClO_4$, battery grade, Sigma-Aldrich) in 30 mL of dry acetonitrile (CH_3CN, anhydrous, Sigma-Aldrich, further dried over columns of activated alumina). The solution was stirred using a magnetic stir bar. All experiments were performed inside an Ar(g)-filled glovebox (< 0.5 ppm of O_2(g)) with an externally connected Biologic SP-300 potentiostat. Photoelectrochemical measurements were collected in the dark and also under 100 mW cm^{-2} of illumination using a three-electrode configuration, with the functionalized silicon substrate as the working electrode, a Pt mesh as the counter electrode, and a Pt wire as the pseudoreference electrode. Illumination was provided by a 300 W ELH-type tungsten-halogen lamp operated at 110 V, and the light intensity was calibrated using a silicon photodiode (Thor Laboratories).

II.D. Data Analysis. Detailed information regarding quantification of the organic overlayer thickness, calculation of the surface recombination velocity (S), and analysis of J–V, J–E, and C_d–V data are presented in the *Supporting Information*.

III. RESULTS AND DISCUSSION

III.A. Synthesis and Characterization of Mixed TFMPA/methyl-terminated Silicon (111) Surfaces.

Covalent functionalization of Si(111) surfaces with mixtures of trifluoromethylphenylacetylene (TFMPA) and methyl moieties was performed using nucleophilic addition chemistry. Following previous literature examples, methylmagnesium chloride (methyl Grignard) was initially used, to passivate sites not terminated by TFMPA (Scheme 1b top row).[11, 18, 20, 27]

Figure 2a shows TIRS data collected at a 74° incident angle for a representative mixed Cl/TFMPA-Si(111) surface synthesized at a reaction temperature, T_{TFMPA}, of 50 °C, before (black, top curve) and after (green, middle curve) methylation with CH_3MgCl. The moderately intense IR peak observed at 1329 cm^{-1} before methylation can be attributed to the vibration of *para*-trifluoromethyl carbons on TFMPA surface moieties ($\nu(CF_3)$) as determined from the simulated FTIR spectrum for gas-phase TFMPA (see *Section II.B.1* for simulation details). An X-ray photoelectron (XP) emission peak at 700 eV (Figure 2b black top curve), corresponding to the F 1*s* signal provided supporting evidence for the presence before methylation of TFMPA moieties on the surface. Prior to methylation, a broad IR band between 1200–1000 cm^{-1}, corresponding primarily to vibrational modes for silicon sub-oxide species,[34] was also observed in the TIRS data. The presence of silicon sub-oxide species on the mixed Cl/TFMPA silicon surface is likely

ascribable to the hydrolysis or oxidation of unreacted Cl-terminated surface sites when the sample was handled under air during insertion into the spectrometers. After methylation with CH_3MgCl, the silicon sub-oxide IR band was absent, and a peak at 1255 cm^{-1} appeared, corresponding to the symmetric bend ("umbrella" mode) for methyl groups on a silicon surface ($\nu(CH_3)$).[20, 34] In combination, these two IR features indicate reaction of unreacted Cl-terminated silicon surface sites to produce Si-CH_3 sites.

After methylation with CH_3MgCl, a substantial reduction was observed in the intensity of the $\nu(CF_3)_{TFMPA}$ IR peak. The decrease of the $\nu(CF_3)_{TFMPA}$ IR peak suggests that during methylation most of the trifluoromethyl groups and/or TFMPA moieties were displaced from the silicon surface. Consistently, XP survey spectra (Figure 2b) for the mixed Cl/TFMPA silicon surface showed a substantial decrease in the intensity of the F 1*s* peak after methylation (green, middle curve), consistent with the displacement of trifluoromethyl groups and/or TFMPA moieties. The surface TFMPA moieties were therefore not fully compatible with the reactivity of CH_3MgCl.

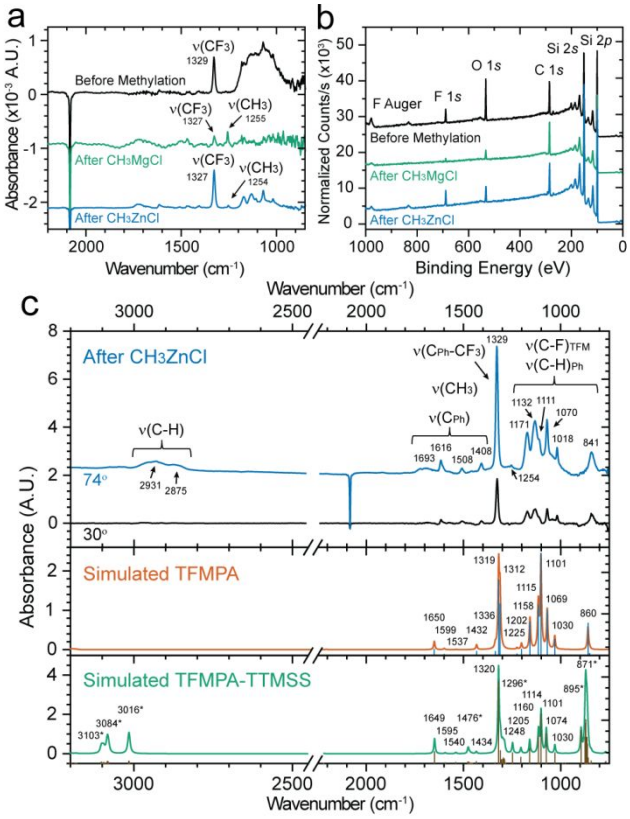

Figure 2. (a) TIR spectra collected at 74 incidence angle and (b) XP survey spectra for a mixed Cl/TFMPA silicon surface before (dark, top curve) and after (green, middle curve) methylation with CH_3MgCl and after (blue bottom curve) methylation with CH_3ZnCl. XPS survey counts were normalized using the intensity of the adventitious C 1*s* peak. The nucleophilic addition of TFMPA was carried out at T_{TFMPA} = 50 °C. (c top panel) TIR spectra collected at 74° (blue, top curve) and 30° (black, bottom curve) incidence angle for a mixed TFMPA/methyl-terminated silicon surface prepared by methylation using CH_3ZnCl, (c middle panel) simulated IR spectrum for TFMPA and (c bottom panel) simulated IR spectrum for TFMPA-functionalized tris(trimethylsilyl)silane (TTMSS) . The TFMPA-TTMSS IR peaks related to vibrational modes for the trimethyl-substituted silanes are labeled with an asterisk. The nucleophilic addition of TFMPA in panel *c* was performed at a higher temperature, T_{TFMPA} = 90 °C, than for panels a and b**.**

Methylzinc chloride (CH_3ZnCl) was then investigated as an alternative route to react with Si-Cl sites that had not been terminated by functionalization with TFMPA. CH_3ZnCl is a milder methylating agent than CH_3MgCl due to the inverse relationship between metal electronegativity and nucleophilicity for methyl-based organometallic reagents (Scheme 1.c). From a theoretical perspective, the larger electronegativity of zinc results in a lower reactivity of CH_3ZnCl than CH_3MgCl towards molecular electrophiles, due to enhanced stabilization of the methyl nucleophile in CH_3ZnCl by comparison to CH_3MgCl. As a consequence of the lower reactivity, the methyl coverage on a silicon surface at a fixed reaction temperature and time is predicted to be lower for CH_3ZnCl than obtained using CH_3MgCl. XPS measurements of Cl-terminated silicon (111) surfaces after methylation with CH_3ZnCl at different reaction temperatures, indicated that ~ 0.99 ML methyl coverage was obtained at a reaction temperature of ~ 180 °C and reaction time of 48 h (Figure S1.b–e).

These reaction conditions for optimal methyl coverage were then used to prepare a mixed Cl/TFMPA silicon surface with CH_3ZnCl. Figure 2a,b show representative TIRS data at a 74° incident angle as well as XP survey spectra of a TFMPA silicon surface before (black, top curve) and after, respectively, methylation with CH_3ZnCl (blue, bottom curve). Methylation with CH_3ZnCl produced no

substantial changes in intensity for the $\nu(CF_3)_{TFMPA}$ peak in the FTIR spectrum or in the F 1*s* peak in the XP survey spectra, indicating that surface TFMPA moieties were not substantially displaced or affected by reacting the surface with CH_3ZnCl. The FTIR spectrum after reaction with CH_3ZnCl also showed the appearance of a $\nu(CH_3)$ peak at 1354 cm^{-1} as well as the absence of a pronounced silicon sub-oxide band, consistent with reaction of Cl-terminated surface sites. Consistently, XP survey spectra for CH_3ZnCl exhibited a substantial decrease in the intensity of the O 1*s* peak in comparison to the surface before methylation.

The reaction temperature of the TFMPA functionalization step, T_{TFMPA} was then increased to facilitate a more detailed FTIR characterization of the mixed Cl/TFMPA silicon surfaces after methylation with CH_3ZnCl. Figure 2c presents the FTIR spectra taken at incidence angles of 74° (top blue curve) and 30° (middle black curve) for a mixed TFMPA/methyl silicon surface functionalized using T_{TFMPA} = 90 °C and CH_3ZnCl. For comparison, the simulated FTIR spectra (see *Section II.B.1* for simulation details) for gas-phase TFMPA (middle panel b) and TFMPA-functionalized tris(trimethylsilyl)silane (TFMPA-TTMSS; bottom panel b) are also displayed. Due to chemical and structural similarities to the active surface site, functionalized tris(trimethylsilyl)silane (TTMSS) was selected as a molecular model to understand the vibrational modes for the functionalized Si(111) surface.[42] A comparison of the experimental results to the simulated FTIR spectra for TFMPA and TFMPA-TTMSS indicated that the IR peaks within the range of ~ 1700–1400 cm^{-1} and 1100–800 cm^{-1} can be attributed to phenyl ring-breathing modes ($\nu(C_{Ph})$) and C-H ($\nu(C\text{-}H)_{Ph}$) coupled with C-F ($\nu(C\text{-}F)_{TFM}$) vibrational modes for TFMPA, respectively. The IR peak at ~ 1239 cm^{-1} can be attributed to the asymmetric stretch between *para*-trifluoromethyl carbons and *para*- phenyl carbons on TFMPA moieties ($\nu(C_{Ph}\text{-}CF_3)_{TFMPA}$). At an incident angle of 30°, all the observed IR peaks decreased substantially in intensity relative to data collected at 74° incidence, indicating that the observed vibrational modes had strong components perpendicular to the surface normal and suggesting that the TFMPA and methyl moieties were preferentially aligned perpendicular to the Si surface.

The chemical composition of mixed TFMPA/methyl-functionalized silicon surfaces was investigated in more detail using high-resolution XPS. Figure 3a–e shows the survey spectra and corresponding C 1*s*, Si 2*p*, F 1*s* and Cl 2*p* high-resolution spectra for a mixed TFMPA/methyl silicon surface functionalized using T_{TFMPA} = 50 °C and CH_3ZnCl. In the C 1*s* spectrum (Figure 3b), peaks ascribable to methyl carbons covalently bonded to surface silicon atoms (at 284 eV (C-Si)[22]) and to surface trifluoromethyl carbons (CF_3) (at 293 eV) provided direct evidence for the presence of methyl and TFMPA moieties on the silicon surface. No detectable amount of silicon oxide, and only the 2*p* doublet ($2p_{3/2}$ and $2p_{1/2}$ peak splitting) corresponding to bulk silicon was observed in the high-resolution Si 2*p* spectrum. The peak at 689 eV in the F 1*s* spectrum, corresponding to covalent fluorine species (F-C), supported the presence of surface trifluoromethyl groups. A weak 2*p* doublet in the Cl 2*p* spectrum indicated the presence of trace amounts (<0.1 monolayer) of unreacted Cl-terminated silicon species on the silicon surface. Considering that TFMPA/methyl silicon surfaces were sonicated in water prior to XPS measurements, the data are consistent with limitations on the coverage of the Si-Cl surface species due to steric hindrance arising from packing constraints.

The thickness of the TFMPA overlayer was determined using the overlayer-attenuation model (Eq. S1) in conjunction with the observed peak areas for CF_3 (C 1*s*), C-Si (C 1*s*) and F-C (F 1*s*). Figure 3f shows the TFMPA overlayer thickness for mixed TFMPA/methyl silicon surfaces synthesized using CH_3ZnCl with TFMPA addition temperatures (T_{TFMPA}) of 50–90 °C (Table S1 for peak-areas and comparison between the CF_3 and F-C peak-area). The results suggest a transition from monolayer to multilayer TFMPA surface coverage at ~ 90 °C, due to the observation of an overlayer thickness greater than the theoretical length for a surface TFMPA moiety (d_{TFMPA} = 2.35 Å; blue dashed line). Note that TFMPA moieties can attenuate the XP emission of CH_3 moieties due to their large difference in height, complicating the determination of the TFMPA:CH_3 ratio at the surface. Since the effects of CH_3 moieties at the Si(111) surface are well understood,[1, 22-23, 38] we focused on understanding the resulting surface properties as function of the TFMPA concentration (or TFMPA overlayer thickness) at the surface.

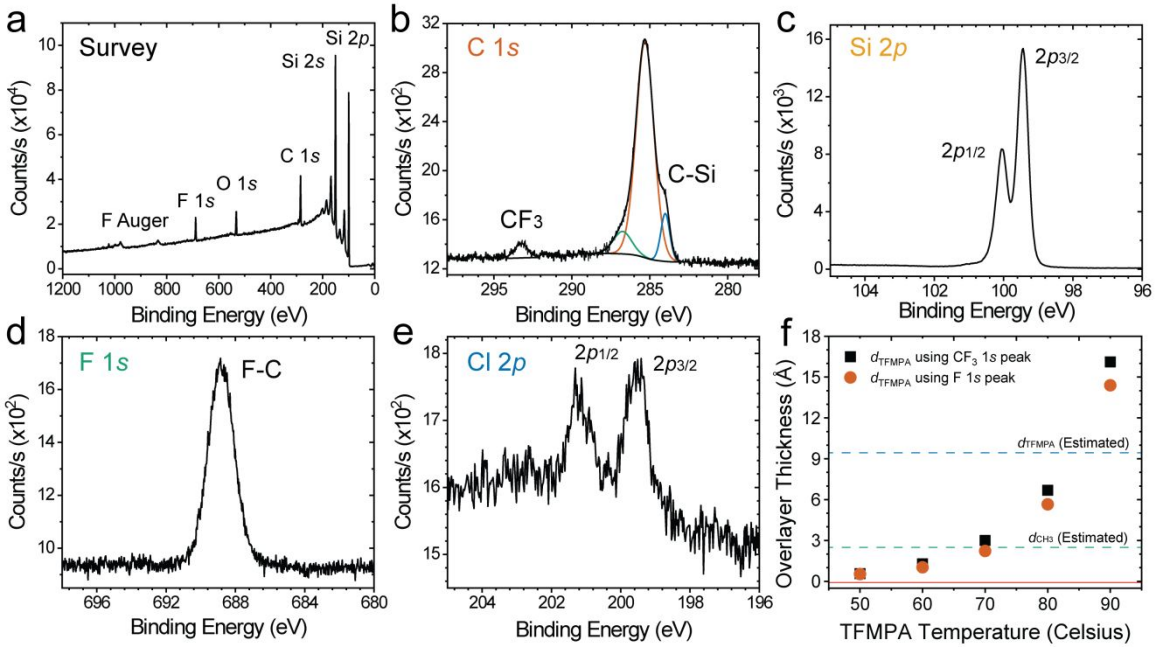

Figure 3. (a) XP survey and corresponding high-resolution spectra for the (b) C 1*s*, (c) Si 2*p*, (d) F 1*s*, and (e) Cl 2*p* regions for a representative mixed TFMPA/methyl-terminated silicon surface. The nucleophilic addition of TFMPA was carried at 50 °C. (f) Summary of overlayer thickness calculations for CF_3 (black symbols) and C-Si (red symbols) species as a function of the TFMPA addition temperature based on the overlayer attenuation model. The overlayer thickness was calculated using both the C 1*s* (black squares) and F 1*s* (orange circles) peaks for CF_3 species of TFMPA.

III.B. Surface Recombination Velocity Measurements by Microwave Conductivity Decay

Figure 4 shows the transient change in microwave conductivity for mixed TFMPA/methyl-terminated silicon surfaces synthesized functionalized using various TFMPA addition temperatures (T_{TFMPA}) with CH_3ZnCl as the methylating agent. For substrates with long bulk charge-carrier lifetimes, changes in the observed lifetimes can be attributed to changes in the surface charge-carrier recombination velocity, *S*.[19, 43] The surface carrier lifetime (τ) is obtained by fitting the transient change in microwave conductivity using a single-exponential decay (see Eq. S2). The corresponding surface recombination velocity is then calculated from the sample thickness (see Eq. S3). Mixed TFMPA/methyl-terminated silicon surfaces (Figure 4, inset) displayed a minimum $S = 205$ cm s^{-1} for $T_{TFMPA} \sim 90$ °C and exhibited a plateau of *S* for functionalization temperatures > 90 °C. The plateau in *S* coincided with the transition from monolayer to multilayer TFMPA coverage observed by XPS, which is consistent with improved surface properties resulting from optimization of the TFMPA-functionalization process. For comparison, CH_3-terminated Si(111) surfaces exhibit $S \sim 20$ cm s^{-1}.[19] The surface recombination velocity is proportional to the concentration of active surface defect states, so the mixed TFMPA/methyl surface at $T_{TFMPA} = 90$ °C displayed a surface defect concentration that was only approximately one order of magnitude larger than that of the well-ordered, well-characterized CH_3-Si(111) surfaces. The *S* behavior of TFMPA/CH_3 surfaces as a function of T_{TFMPA} is in contrast with that of TFPA/CH_3 surfaces,[11] which exhibit an increase in *S* with an increase in the concentration of TFPA moieties at the surface. Thus, the *S* results for TFMPA/CH_3-Si(111) suggest that a lower concentration of surface states (in comparison to TFPA) can be achieved due to a denser packing of moieties and/or more effective blocking of reactive sites at the surface.

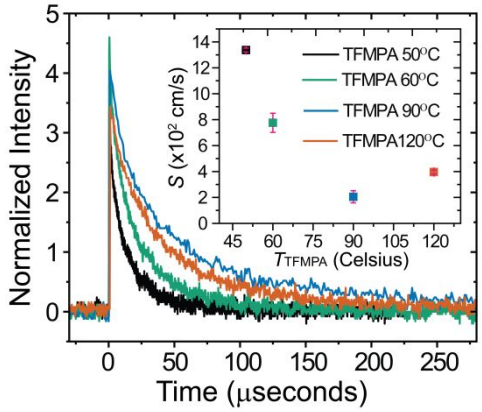

Figure 4. Time-resolved microwave conductivity measurements for mixed TFMPA/methyl-terminated silicon surfaces prepared by nucleophilic addition of TFMPA at 50 (black), 60 (green), 90 (blue) and 120 (red) °C. Inset figure is a summary of the average surface recombination velocity (S) as a function of the TFMPA addition temperature (T_{TFMPA}), averaged over six samples.

III.C. Reversal of the functionalization steps

With CH_3ZnCl as the methylating agent, TFMPA/methyl-terminated silicon (111) surfaces were also prepared by methylation followed by nucleophilic addition of TFMPA (*Section SIII*). This alternative ordering of the reaction steps was enabled due to the milder reactivity of CH_3ZnCl relative to CH_3MgCl, which allowed controllable partial methylation of the Cl-terminated silicon surface (Figure S1). The resulting mixed methyl/Cl surfaces were then reacted with a nucleophile such as TFMPA magnesium chloride to yield a mixed TFMPA/methyl-terminated silicon surface (Figure S2 and Figure S3). The ability to alter the order of the reaction steps prevented exposure of the desired chemical functionalities of a nucleophile of interest to harsh methylating conditions. Consequently, partial methylation using CH_3ZnCl would enable functionalization of Si using a wide range of nucleophilic moieties that are chemically incompatible with methylating agents and reaction conditions.

III.D. Properties of junctions between Hg and mixed TFMPA/methyl silicon surfaces

Figure 5a displays the current density (J) versus voltage (V) behavior for mixed TFMPA/methyl-terminated p-Si surfaces synthesized using various TFMPA addition temperatures (T_{TFMPA}) with CH_3ZnCl as the methylating agent. For comparison, the J-V behavior of p-type H-Si(111) and p-type CH_3-Si(111) terminated surfaces are also presented.

For p-type CH_3-Si(111) electrodes, the $ln(J)$ vs. V characteristic was symmetric along the y-axis, indicating an ohmic response (i.e. a plot of J vs. V was linear). The ohmic response is consistent with accumulation under equilibrium conditions of majority charge carriers (holes) at the semiconductor surface and within the space-charge region. The surface Fermi level of p-type CH_3-Si(111) before equilibration is thus above (at a more negative potential) the work function of Hg (~4.45 eV versus vacuum; Figure 6a). In contrast p-type H-Si(111) electrodes displayed asymmetric $ln(J)$–V behavior along the y-axis, indicating current rectification. This diode-like junction is indicative of downwards band bending at equilibrium, which results in depletion of majority charge carriers under equilibration conditions near the surface and within the space-charge region. Hence, before equilibration the surface Fermi level of p-type H-Si(111) is below (at a more positive potential) the work function of Hg (Figure 6b). Thus, the band positions for H-terminated silicon shifted toward positive potentials relative to the band-edge potentials of CH_3-terminated silicon, consistent with H-termination producing a more positive dipole layer than CH_3-termination (Figure 6) at the silicon surface.

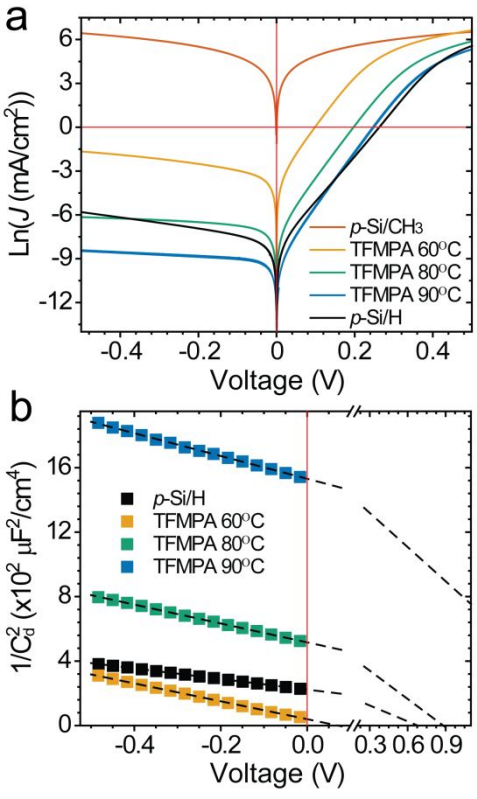

Figure 5. Electrical characterization of mixed TFMPA/methyl-terminated p-Si surfaces in contact with a Hg drop. (a) Natural logarithm of the current density vs applied voltage (ln J vs V) and (b) Mott-Schottky (capacitance vs applied voltage; $1/C_d^2$ vs V) plots for T_{TFMPA} = 60, 80 or 90 °C, in comparison to methyl- and hydrogen-terminated p-Si(111) surfaces

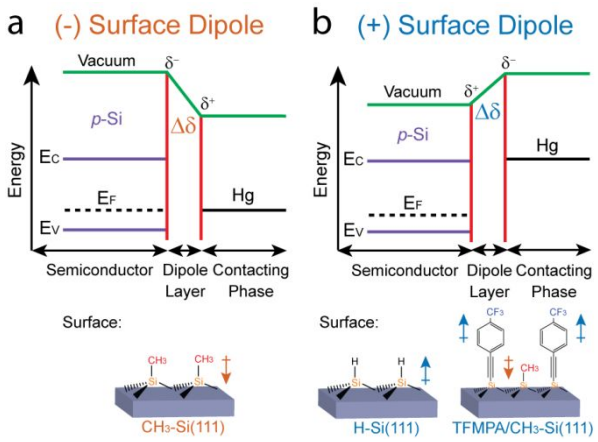

Figure 6. Energy-band diagram illustrating the shift induced by (a) negative and (b) positive dipole layers on the vacuum energy across the interface between p-Si and a Hg contact. In this figure, $\mathbf{E}_C$, $\mathbf{E}_V$, and $\mathbf{E}_F$ represent the energies of the conduction-band edge, valence-band edge, and Fermi levels, respectively, for p-Si. The vacuum-energy shift caused by the electric field within the dipole layer is represented as Δδ. Methyl- (CH_3-Si(111)), hydrogen- (H-Si(111)) and TFMPA/methyl- (TFMPA/CH_3-Si(111)) terminated p-silicon surfaces are shown as examples of negative and positive dipole layers, respectively, arising from surface functionalization.

Mixed TFMPA/methyl p-Si electrodes showed a rectifying (diode) *ln*(*J*)–*V* response, analogous to p-type H-Si(111) electrodes and in contrast to the ohmic response observed for p-type CH_3-Si(111) (Figure 5a), consistent with the existence of a depletion space-charge region in contact with Hg. Assuming that the current is limited by thermionic emission, the *y*-intercept of the linear region observed in the *ln*(*J*)–*V* under positive applied potential (forward bias) can be used to obtain the barrier height, ϕ, at the junction (see Eq. S4). Barrier heights calculated from analysis of *ln*(*J*)–*V* data for mixed TFMPA/CH_3-terminated p-Si(111) electrodes increased as T_{TFMPA} increased (Table 1). The concentration of surface TFMPA moieties as observed using XPS also increased with increasing T_{TFMPA}, consistent with expectations for an increase in the magnitude of the positive surface dipole produced by surface TFMPA moieties. The barrier height for mixed TFMPA/CH_3-terminated p-Si(111) electrodes made at T_{TFMPA} = 90 °C was equal to or slightly greater than the barrier height of p-type H-Si(111) electrodes with Hg. Consequently, *ln*(*J*)–*V* measurements under forward bias suggest that the magnitude of the positive surface dipole induced by surface TFMPA moieties produced using T_{TFMPA} = 90 °C approached that of a H-terminated surface.

The barrier height of the Hg junction was also investigated using impedance spectroscopy to determine the differential capacitance (C_d) for the functionalized p-Si(111) electrodes under negative applied bias (reverse bias) (Figure 5b). The differential capacitance was obtained by fitting the impedance response at discrete steps in applied voltage using a simplified Randles circuit ($R_1 + C_d/R_2$). For an ideal metal/semiconductor junction under reverse bias, changes in C_d can be attributed to changes in the width of the depletion region and are described by Mott-Schottky equation (Eq. S5). The flat-band voltage can be obtained from the *x*-intercept of a linear fit to the data when $1/C_d^2$ is plotted vs *V*. The barrier height of the junction can then be calculated for a p-type semiconductor by adding the potential difference between the bulk Fermi level and the valence-band edge (Eq. S6). A linear response was observed for $1/C_d^2$ vs *V* for all the functionalized p-Si electrodes (Figure 5b), as expected based on the Mott-Schottky equation.

Figure 5b compares the $1/C_d^2$ versus *V* data for the mixed TFMPA/methyl-terminated p-Si(111) electrodes with the behavior of p-type H-Si(111)/Hg contacts. The *x*-intercept at T_{TFMPA} = 60 °C and 80 °C, and consequently the flat-band voltage (V_{FB}) and the barrier height (ϕ_{CV}), increased as T_{TFMPA} increased, in agreement with the trend in barrier height observed from *ln*(*J*)–*V* measurements. A substantial quantitative difference was observed for T_{TFMPA} = 60 °C between the values obtained from the *ln*(*J*)–*V* and $1/C_d^2$–*V* measurements. The electrical transport properties of semiconductor/overlayer/metal junctions can be simultaneously dominated by thermionic emission and tunneling through the organic overlayer.[44-45] The thermionic emission barrier is directly proportional to the band bending in the semiconductor, whereas the tunneling barrier is determined by the difference between the semiconductor band edges and the HOMO and LUMO of the organic overlayer.[46] Considering that *ln*(*J*)–*V* is a direct measurement of the interfacial charge transfer and $1/C_d^2$–*V* is related to the capacitance of the components in the junction, discrepancies between these two types of measurements could result from a contribution from tunneling to the electrical transport properties of the junction.[44-45] In contrast, H-terminated p-Si(111), which is an atomically flat and has simple termination, shows close quantitative agreement between the barrier height values obtained by these two types of measurements.

At T_{TFMPA} = 90 °C, the *x*-intercept further increased reaching values substantially larger than the band gap of silicon (1.12 eV), which indicates that the TFMPA overlayer for this reaction condition displays a behavior similar to that of a thin insulating overlayer. It has been previously demonstrated that the presence of thin insulating overlayers modifies the *x*-intercept of the Mott-Schottky equation, such that the *x*-intercept is instead directly proportional to $V_{FB} + V_L$, where V_L is a constant emerging from the additional series capacitance of the thin insulating overlayer (details in *Section I.E* and *Section IV* of the *Supporting Information*).[47-48] Thus, linear $1/C_d^2$–*V* responses with *x*-intercept values substantially larger than the band gap of silicon are indicative of the presence of a non-negligible organic overlayer capacitance. Although V_{FB} and ϕ_{CV} cannot be directly determined without prior knowledge of the

organic insulating overlayer capacitance, the T_{TFMPA} = 90 °C results are indicative of multilayer-like thickness values and an overall positive electric field (dipole moment) for the TFMPA overlayer. In addition, the slightly insulating behavior observed at T_{TFMPA} = 90 °C is consistent with the transition from monolayer to multilayer thickness values observed by XPS in Figure 3f. The overall dependence of the $1/C_d^2$–V response with T_{TFMPA} obtained for the mixed TFMPA/methyl-terminated p-Si(111) electrodes using impedance spectroscopy provides evidence consistent with expectations for a positive surface dipole when Si is functionalized with TFMPA moieties.

Table 1. Barrier heights (ϕ) obtained for the functionalized p-Si(111) electrodes in contact with Hg (Figure 5a,b). Values for the average and standard deviation for three electrodes are provided in parenthesis.

p-type Sample	ϕ_{JV} (mV)	N_D (× 10^{16} cm^{-3})	*x*-Intercept (mV)	ϕ_{CV} (mV)
TFMPA/CH_3-Si T_{TFMPA} = 60 °C	650 (661 ± 7)	2.14 (2.09 ± 0.08)	70 (75 ± 14)	255 (259 ± 13)
TFMPA/CH_3-Si T_{TFMPA} = 80 °C	716 (734 ± 12)	2.04 (2.16 ± 0.14)	884 (907 ± 23)	1069 (1080 ± 21)
TFMPA/CH_3-Si T_{TFMPA} = 90 °C	785 (798 ± 10)	1.68 (1.88 ± 0.26)	2152 (3330 ± 338)	N/A
H-Si	770 (754 ± 8)	3.65 (3.65 ± 0.06)	683 (676 ± 6)	843 (836 ± 6)

III.E. Photoelectrochemical Response of TFMPA/methyl-terminated Si(111) surfaces.

Figure 7 shows the V_{oc} for mixed TFMPA/methyl-terminated p-Si(111) electrodes functionalized using T_{TFMPA} = 60 °C and T_{TFMPA} = 90 °C, as a function of the effective solution potential. For comparison, the behavior of p-type CH_3-Si(111) electrodes is also presented. Note that in Figure 7 the concentration of the minority-carrier scavenger redox species was normalized to 10 mM by converting the measured cell potential (E(A/A$^-$)) to an effective solution potential (E_{eff}(A/A$^-$) (see *Section SID*).[38]

Under 100 mW cm^{-2} of simulated solar illumination, TFMPA/methyl-terminated p-Si(111) electrodes exhibited a linear V_{oc} response to E_{eff}(A/A$^-$) and moreover the response shifted to larger V_{oc} values (positive shift) relative to the behavior of p-type CH_3-Si(111) electrodes, ΔV_{oc}. The ΔV_{oc} shifts for TFMPA/methyl-terminated p-Si(111) electrodes were larger for T_{TFMPA} = 90 °C than for T_{TFMPA} = 60 °C, indicating a correlation between the magnitude of the positive increase in surface dipole and the concentration of surficial TFMPA moieties. The largest ΔV_{oc} was observed for the $(CpCO_2CH_3)_2Co^{+/0}$ redox couple, at an effective solution potential of -0.66 V versus ferrocenium/ferrocene ($Fc^{+/0}$), which produced ΔV_{oc} ~ 150 mV for p-Si(111) electrodes functionalized using T_{TFMPA} = 90 °C. A similar shift was also observed for the flat-band potential (E_{fb}) obtained from Mott-Schottky measurements of the TFMPA/methyl-Si electrodes in contact with $(CpCO_2CH_3)_2Co^{+/0}$ (Figure S5 and Table S2). The magnitude of ΔV_{oc} gradually decreased as E_{eff}(A/A$^-$) became more negative. For example, for the Cp_2*$Co^{+/0}$ redox couple having E_{eff}(A/A$^-$) -1.32 V versus $Fc^{+/0}$, ΔV_{oc} was ~ 40 mV. Surface states can decrease the magnitude of the slope of the V_{oc} response through mechanisms such as Fermi-level pinning and surface carrier recombination, hence a smaller slope of V_{oc} vs E_{eff}(A/A$^-$) correspond to a higher surface defect-state concentration and the observed trend is in agreement with the S data obtained for TFMPA/methyl-terminated surfaces (Figure 4).

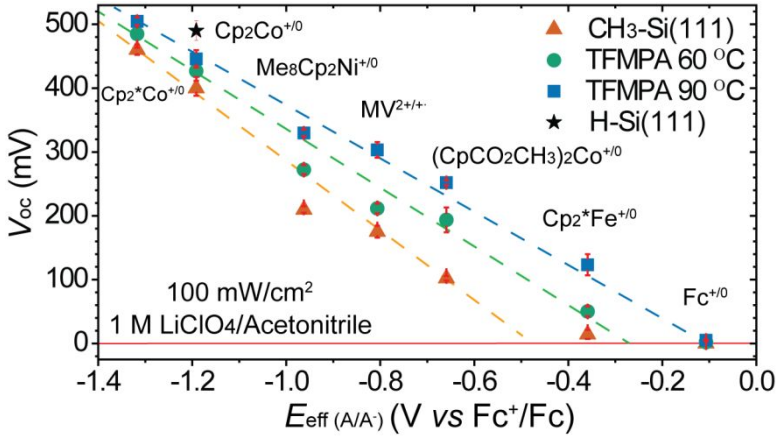

Figure 7. Open-circuit voltage (V_{oc}) of mixed TFMPA/methyl-terminated p-Si(111) electrodes submerged in acetonitrile electrolytes containing 1.0 M $LiClO_4$ and under 100 mW cm^{-2} (1 Sun) illumination. V_{oc} values are shown as a function of the effective solution potential (E_{eff}) for TFMPA addition temperatures of 60 °C (green circles) and 90 °C (blue squares), in comparison to a methyl-terminated p-Si(111)

(red triangles). Each V_{oc} data point is the averaged result from 2–3 electrodes constructed from four reaction batches. The V_{oc} for hydrogen-terminated p-Si(111) (black star) using cobaltocene$^{+/0}$ as the redox couple has been included as an additional control.

The photoelectrochemical response of mixed TFMPA/methyl-terminated silicon surfaces in CH_3CN was investigated further by evaluating the characteristics under illumination. Figure 8a,b shows the current density (J) versus applied potential (E) behavior for representative mixed TFMPA/methyl-functionalized p-Si electrodes using $(CpCO_2CH_3)_2Co^{+/0}$ and/or $Cp_2Co^{+/0}$ as the redox couples. For comparison, the behavior of p-type CH_3-Si(111) and p-type H-Si(111) electrodes is also presented. Mutually similar photocurrent plateaus were observed for all of the functionalized electrodes under negative applied potentials, indicating similar light transmittance across all the functionalized layers. Notably, for some redox couples, the largest observed photovoltage was obtained from mixed TFMPA/methyl-functionalized photocathodes. This behavior contrasts with that of TFPA/CH_3-functionalized p-Si(111),[11] which yielded an increased barrier height but lower photovoltages than p-type CH_3-Si(111) and p-type H-Si(111) photocathodes. Mixed TFMPA/methyl-terminated electrodes displayed a lower fill factor than p-type CH_3-Si(111) electrodes, especially in contact with $Cp_2Co^{+/0}$. Surface states can lower the fill factor through surface recombination, so the decrease in fill factor is consistent with the higher S for the mixed TFMPA/methyl-terminated surface relative to p-type CH_3-Si(111). Consequently, a further reduction in the rates of charge-carrier recombination at the surface of mixed TFMPA/methyl-terminated silicon is required to take full advantage of the increase in V_{oc} caused by the positive band-edge shift (positive surface dipole) that accompanies TFMPA functionalization.

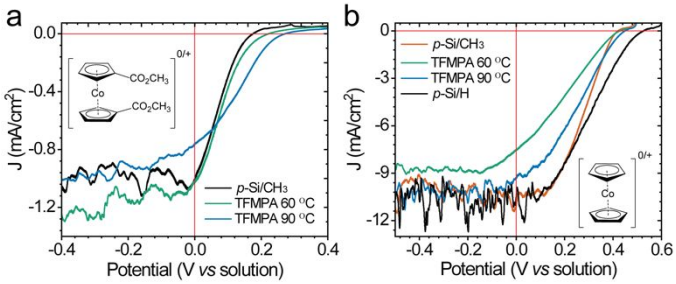

Figure 8. *J-E* characteristics for representative TFMPA/methyl-, methyl-, and hydrogen-terminated p-Si(111) electrodes using (a) dicarbomethoxycobaltocene$^{+/0}$ and (b) cobaltocene$^{+/0}$ as redox couples.

IV. CONCLUSIONS

Covalent functionalization of silicon (111) with mixtures of 4-trifluoromethylphenylacetylene (TFMPA) and methyl moieties provides a wet-chemical approach to introducing a positive surface dipole while retaining a surface with a high degree of electrical surface passivation. XPS and TIRS measurements indicated that methylation using CH_3MgCl resulted in displacement of trifluoromethyl or TFMPA moieties from the surface. However, methylation of Si using CH_3ZnCl, a milder and more controllable reagent, yielded mixed TFMPA/CH_3-terminated p-Si(111) occurred without substantially changing the concentration of surface TFMPA species. The mild reactivity of CH_3ZnCl also enabled mixed TFMPA/methyl functionalization through initial partial methylation of the Cl-terminated surface and subsequent nucleophilic addition of TFMPA. This alternative ordering of reaction steps allows for molecules of interest to be covalently attached to the Si(111) surface without subsequent exposure to the methylation reaction, and allows the incorporation on Si(111) of functional groups that are susceptible to nucleophilic attack.

Mixed TFMPA/methyl-functionalized p-Si(111) surfaces had surface recombination velocities as low as 2.0×10^2 cm s^{-1}, only one order of magnitude larger than completely methyl-terminated Si(111) surfaces. TFMPA induced a positive surface dipole with a magnitude that scaled with the concentration of surface TFMPA moieties. The positive surface dipole resulted in an increase in V_{oc} of up to ~ 150 mV relative to methyl-terminated p-Si(111) electrodes. However, realization of the full benefits of molecular-level control of the band alignment across a semiconductor/electrolyte junction, as supported by the increase in V_{oc} obtained through mixed TFMPA/methyl functionalization of p-Si(111) demonstrated herein, requires approaches to further improve fill factors and further passivate surface defects.

ASSOCIATED CONTENT

SUPPORTING INFORMATION

The Supporting Information is available free of charge on the ACS Publications website.

Data analysis equations, characterization data for CH_3-Si(111) surfaces prepared using methylzinc chloride and for methyl/TFMPA-terminated Si surfaces, Bode plot comparison for H- and methyl- terminated p-Si(111) in contact with Hg, and Mott-Schottky plots for TFMPA/methyl-terminated p-Si electrodes in contact with $(CpCO_2CH_3)_2Co^{+/0}$.

AUTHORS INFORMATION

Corresponding Author

*E-mail: nslewis@caltech.edu. Tel: (626) 395-6335.

Notes

The authors declare no competing financial interest.

ACKNOWLEDGEMENTS

M.C. acknowledges support from the Ford Foundation under the Postdoctoral Scholar Fellowship program. B.S.B. and M.C. acknowledge support from the National Science Foundation CCI Solar Fuels Program under Grant No. CHE-1305124. N.S.L. and M.C. acknowledges support from the National Science Foundation under Grant No. CHE-1808599. Instrumentation support was provided by the Molecular Materials Resource Center of the Beckman Institute at the California Institute of Technology.

V. REFERENCES

(1) Li, Y.; O'Leary, L. E.; Lewis, N. S.; Galli, G. Combined Theoretical and Experimental Study of Band-Edge Control of Si through Surface Functionalization. *J. Phys. Chem. C* **2013**, *117*, 5188−5194.

(2) Gleason-Rohrer, D. C.; Brunschwig, B. S.; Lewis, N. S. Measurement of the Band Bending and Surface Dipole at Chemically Functionalized Si(111)/Vacuum Interfaces. *J. Phys. Chem. C* **2013**, *117*, 18031−18042.

(3) Hartig, P.; Dittrich, T.; Rappich, J. Surface Dipole Formation and Non-Radiative Recombination at P-Si(111) Surfaces During Electrochemical Deposition of Organic Layers. *J. Electroanal. Chem.* **2002**, *524-525*, 120−126.

(4) Wick-Joliat, R.; Musso, T.; Prabhakar, R. R.; Löckinger, J.; Siol, S.; Cui, W.; Sévery, L.; Moehl, T.; Suh, J.; Hutter, J., et al. Stable and Tunable Phosphonic Acid Dipole Layer for Band Edge Engineering of Photoelectrochemical and Photovoltaic Heterojunction Devices. *Energy Environ. Sci.* **2019**, *12*, 1901−1909.

(5) Har-Lavan, R.; Schreiber, R.; Yaffe, O.; Cahen, D. Molecular Field Effect Passivation: Quinhydrone/Methanol Treatment of N-Si(100). *J. Appl. Phys.* **2013**, *113*, 084909.

(6) Walter, M. G.; Warren, E. L.; McKone, J. R.; Boettcher, S. W.; Mi, Q.; Santori, E. A.; Lewis, N. S. Solar Water Splitting Cells. *Chem. Rev.* **2010**, *110*, 6446−6473.

(7) Choi, K.; Buriak, J. M. Hydrogermylation of Alkenes and Alkynes on Hydride-Terminated Ge(100) Surfaces. *Langmuir* **2000**, *16*, 7737−7741.

(8) Hilal, H. S.; Turner, J. A. Controlling Charge-Transfer Processes at Semiconductor/Liquid Junctions. *Electrochim. Acta* **2006**, *51*, 6487−6497.

(9) Kim, H. J.; Seo, J.; Rose, M. J. H_2 Photogeneration Using a Phosphonate-Anchored Ni-Pnp Catalyst on a Band-Edge-Modified *P*-Si(111)|Azo Construct. *ACS Appl. Mater. Interfaces* **2016**, *8*, 1061−1066.

(10) Seo, J.; Kim, H. J.; Pekarek, R. T.; Rose, M. J. Hybrid Organic/Inorganic Band-Edge Modulation of *P*-Si(111) Photoelectrodes: Effects of R, Metal Oxide, and Pt on H_2 Generation. *J. Am. Chem. Soc.* **2015**, *137*, 3173−3176.

(11) Plymale, N. T.; Ramachandran, A. A.; Lim, A.; Brunschwig, B. S.; Lewis, N. S. Control of the Band-Edge Positions of Crystalline Si(111) by Surface Functionalization with 3,4,5-Trifluorophenylacetylenyl Moieties. *J. Phys. Chem. C* **2016**, *120*, 14157−14169.

(12) Lasseter, T. L.; Clare, B. H.; Abbott, N. L.; Hamers, R. J. Covalently Modified Silicon and Diamond Surfaces: Resistance to Nonspecific Protein Adsorption and Optimization for Biosensing. *J. Am. Chem. Soc.* **2004**, *126*, 10220−10221.

(13) Garner, L. E.; Steirer, K. X.; Young, J. L.; Anderson, N. C.; Miller, E. M.; Tinkham, J. S.; Deutsch, T. G.; Sellinger, A.; Turner, J. A.; Neale, N. R. Covalent Surface Modification of Gallium Arsenide Photocathodes for Water Splitting in Highly Acidic Electrolyte. *ChemSusChem* **2017**, *10*, 767−773.

(14) Pujari, S. P.; Scheres, L.; Marcelis, A. T. M.; Zuilhof, H. Covalent Surface Modification of Oxide Surfaces. *Angewandte Chemie International Edition* **2014**, *53*, 6322−6356.

(15) MacLeod, B. A.; Steirer, K. X.; Young, J. L.; Koldemir, U.; Sellinger, A.; Turner, J. A.; Deutsch, T. G.; Olson, D. C. Phosphonic Acid Modification of $Gainp_2$ Photocathodes toward Unbiased Photoelectrochemical Water Splitting. *ACS Appl. Mater. Interfaces* **2015**, *7*, 11346−11350.

(16) Kocha, S. S.; Turner, J. A. Displacement of the Bandedges of $Gainp_2$ in Aqueous Electrolytes Induced by Surface Modification. *J. Electrochem. Soc.* **1995**, *142*, 2625−2630.

(17) Tan, M. X.; Laibinis, P. E.; Nguyen, S. T.; Kesselman, J. M.; Stanton, C. E.; Lewis, N. S. Principles and Applications of Semiconductor Photoelectrochemistry. *Prog. Inorg. Chem.* **1994**, *41*, 21−144.

(18) Bansal, A.; Li, X.; Lauermann, I.; Lewis, N. S.; Yi, S. I.; Weinberg, W. H. Alkylation of Si Surfaces Using a Two-Step Halogenation/Grignard Route. *J. Am. Chem. Soc.* **1996**, *118*, 7225−7226.

(19) Royea, W. J.; Juang, A.; Lewis, N. S. Preparation of Air-Stable, Low Recombination Velocity Si(111) Surfaces through Alkyl Termination. *Appl. Phys. Lett.* **2000**, *77*, 1988−1990.

(20) O'Leary, L. E.; Johansson, E.; Brunschwig, B. S.; Lewis, N. S. Synthesis and Characterization of Mixed Methyl/Allyl Monolayers on Si(111). *J. Phys. Chem. B* **2010**, *114*, 14298−14302.

(21) Plymale, N. T.; Kim, Y.-G.; Soriaga, M. P.; Brunschwig, B. S.; Lewis, N. S. Synthesis, Characterization, and Reactivity of Ethynyl- and Propynyl-Terminated Si(111) Surfaces. *J. Phys. Chem. C* **2015**, *119*, 19847−19862.

(22) Webb, L. J.; Nemanick, E. J.; Biteen, J. S.; Knapp, D. W.; Michalak, D. J.; Traub, M. C.; Chan, A. S. Y.; Brunschwig, B. S.; Lewis, N. S. High-Resolution X-Ray Photoelectron Spectroscopic Studies of Alkylated Silicon(111) Surfaces. *J. Phys. Chem. B* **2005**, *109*, 3930−3937.

(23) Maldonado, S.; Plass, K. E.; Knapp, D.; Lewis, N. S. Electrical Properties of Junctions between Hg and Si(111) Surfaces Functionalized with Short-Chain Alkyls. *J. Phys. Chem. C* **2007**, *111*, 17690−17699.

(24) Maldonado, S.; Knapp, D.; Lewis, N. S. Near-Ideal Photodiodes from Sintered Gold Nanoparticle Films on Methyl-Terminated Si(111) Surfaces. *J. Am. Chem. Soc.* **2008**, *130*, 3300−3301.

(25) Maldonado, S.; Lewis, N. S. Behavior of Electrodeposited Cd and Pb Schottky Junctions on Ch_3-Terminated N-Si(111) Surfaces. *J. Electrochem. Soc.* **2009**, *156*, H123−H128.

(26) Lattimer, J. R. C.; Brunschwig, B. S.; Lewis, N. S.; Gray, H. B. Redox Properties of Mixed Methyl/Vinylferrocenyl Monolayers on Si(111) Surfaces. *J. Phys. Chem. C* **2013**, *117*, 27012−27022.

(27) O'Leary, L. E.; Rose, M. J.; Ding, T. X.; Johansson, E.; Brunschwig, B. S.; Lewis, N. S. Heck Coupling of Olefins to Mixed Methyl/Thienyl Monolayers on Si(111) Surfaces. *J. Am. Chem. Soc.* **2013**, *135*, 10081−10090.

(28) Johansson, E.; Boettcher, S. W.; O'Leary, L. E.; Poletayev, A. D.; Maldonado, S.; Brunschwig, B. S.; Lewis, N. S. Control of the Ph-Dependence of the Band Edges of Si(111) Surfaces Using Mixed Methyl/Allyl Monolayers. *J. Phys. Chem. C* **2011**, *115*, 8594−8601.

(29) Kearney, K.; Iyer, A.; Rockett, A.; Staykov, A.; Ertekin, E. Effect of Surface Coverage and Composition on the Stability and Interfacial Dipole of Functionalized Silicon. *J. Phys. Chem. C* **2017**, *121*, 11312−11318.

(30) Nemanick, E. J.; Hurley, P. T.; Brunschwig, B. S.; Lewis, N. S. Chemical and Electrical Passivation of Silicon (111) Surfaces through Functionalization with Sterically Hindered Alkyl Groups. *J. Phys. Chem. B* **2006**, *110*, 14800−14808.

(31) Higashi, G. S.; Chabal, Y. J.; Trucks, G. W.; Raghavachari, K. Ideal Hydrogen Termination of the Si (111) Surface. *Appl. Phys. Lett.* **1990**, *56*, 656−658.

(32) Wade, C. P.; Chidsey, C. E. D. Etch-Pit Initiation by Dissolved Oxygen on Terraces of H-Si(111). *Appl. Phys. Lett.* **1997**, *71*, 1679−1681.

(33) Rivillon, S.; Chabal, Y. J.; Webb, L. J.; Michalak, D. J.; Lewis, N. S.; Halls, M. D.; Raghavachari, K. Chlorination of Hydrogen-Terminated Silicon (111) Surfaces. *J. Vac. Sci. Technol. A* **2005**, *23*, 1100−1106.

(34) Webb, L. J.; Rivillon, S.; Michalak, D. J.; Chabal, Y. J.; Lewis, N. S. Transmission Infrared Spectroscopy of Methyl- and Ethyl-Terminated Silicon(111) Surfaces. *J. Phys. Chem. B* **2006**, *110*, 7349−7356.

(35) Schmidt, M. W.; Baldridge, K. K.; Boatz, J. A.; Elbert, S. T.; Gordon, M. S.; Jensen, J. H.; Koseki, S.; Matsunaga, N.; Nguyen, K. A.; Su, S., et al. General Atomic and Molecular Electronic Structure System. *J. Comput. Chem.* **1993**, *14*, 1347−1363.

(36) Gordon, M. S.; Schmidt, M. W. *Theory and Applications of Computational Chemistry: The First Forty Years*; Elsevier: Amsterdam, 2005.

(37) O'boyle, N. M.; Tenderholt, A. L.; Langner, K. M. Cclib: A Library for Package-Independent Computational Chemistry Algorithms. *J. Comput. Chem.* **2008**, *29*, 839−845.

(38) Grimm, R. L.; Bierman, M. J.; O'Leary, L. E.; Strandwitz, N. C.; Brunschwig, B. S.; Lewis, N. S. Comparison of the Photoelectrochemical Behavior of H-Terminated and Methyl-Terminated Si(111) Surfaces in Contact with a Series of One-Electron, Outer-Sphere Redox Couples in Ch_3cn. *J. Phys. Chem. C* **2012**, *116*, 23569−23576.

(39) Hart, W. P.; Macomber, D. W.; Rausch, M. D. A New, General Route to Functionally Substituted .Eta.5-Cyclopentadienyl Metal Compounds. *J. Am. Chem. Soc.* **1980**, *102*, 1196−1198.

(40) Sheats, J. E.; Rausch, M. D. Synthesis and Properties of Cobalticinium Salts. I. Synthesis of Monosubstituted Cobalticinium Salts. *J. Org. Chem.* **1970**, *35*, 3245−3249.

(41) Megehee, E. G.; Johnson, C. E.; Eisenberg, R. Optical Versus Thermal Electron Transfer between Iridium(I) Maleonitriledithiolate Complexes and Methyl Viologen. *Inorg. Chem.* **1989**, *28*, 2423−2431.

(42) Rijksen, B.; van Lagen, B.; Zuilhof, H. Mimicking the Silicon Surface: Reactivity of Silyl Radical Cations toward Nucleophiles. *J. Am. Chem. Soc.* **2011**, *133*, 4998−5008.

(43) Brenot, R.; Vanderhaghen, R.; Drevillon, B.; French, I.; Roca i Cabarrocas, P. Time Resolved Microwave Conductivity Measurements for the Characterization of Transport Properties in Thin Film Micro-Crystalline Silicon. *Thin Solid Films* **1997**, *296*, 94−97.

(44) Salomon, A.; Boecking, T.; Seitz, O.; Markus, T.; Amy, F.; Chan, C.; Zhao, W.; Cahen, D.; Kahn, A. What Is the Barrier for Tunneling through Alkyl Monolayers? Results from N- and P-Si−Alkyl/Hg Junctions. *Adv. Mater.* **2007**, *19*, 445−450.

(45) Segev, L.; Salomon, A.; Natan, A.; Cahen, D.; Kronik, L.; Amy, F.; Chan, C. K.; Kahn, A. Electronic Structure of Si(111)-Bound Alkyl Monolayers: Theory and Experiment. *Phys. Rev. B* **2006**, *74*, 165323.

(46) Cahen, D.; Kahn, A. Electron Energetics at Surfaces and Interfaces: Concepts and Experiments. *Adv. Mater.* **2003**, *15*, 271−277.

(47) Cardon, F.; Gomes, W. P. On the Determination of the Flat-Band Potential of a Semiconductor in Contact with a Metal or an Electrolyte from the Mott-Schottky Plot. *J. Phys. D: Appl. Phys.* **1978**, *11*, L63−L67.

(48) Sze, S. M.; Ng, K. K. *Physics of Semiconductor Devices*; John Wiley & Sons, Inc., 2006.

TOC Graphic:

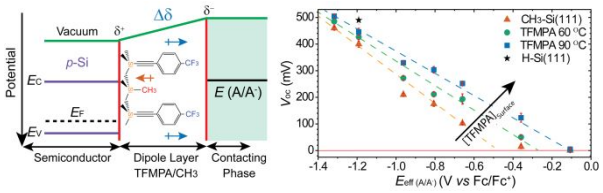
Vacuum
Δδ
δ+
δ-
p-Si
Potential
Ec
EF
Ev
E (A/A-)
Semiconductor
Dipole Layer
TFMPA/CH3
Contacting
Phase
CH3-Si(111)
TFMPA 60 °C
TFMPA 90 °C
H-Si(111)
Vsc (mV)
[TFMPA]surface
Eeff (A/A-) (V vs Fc/Fc+)